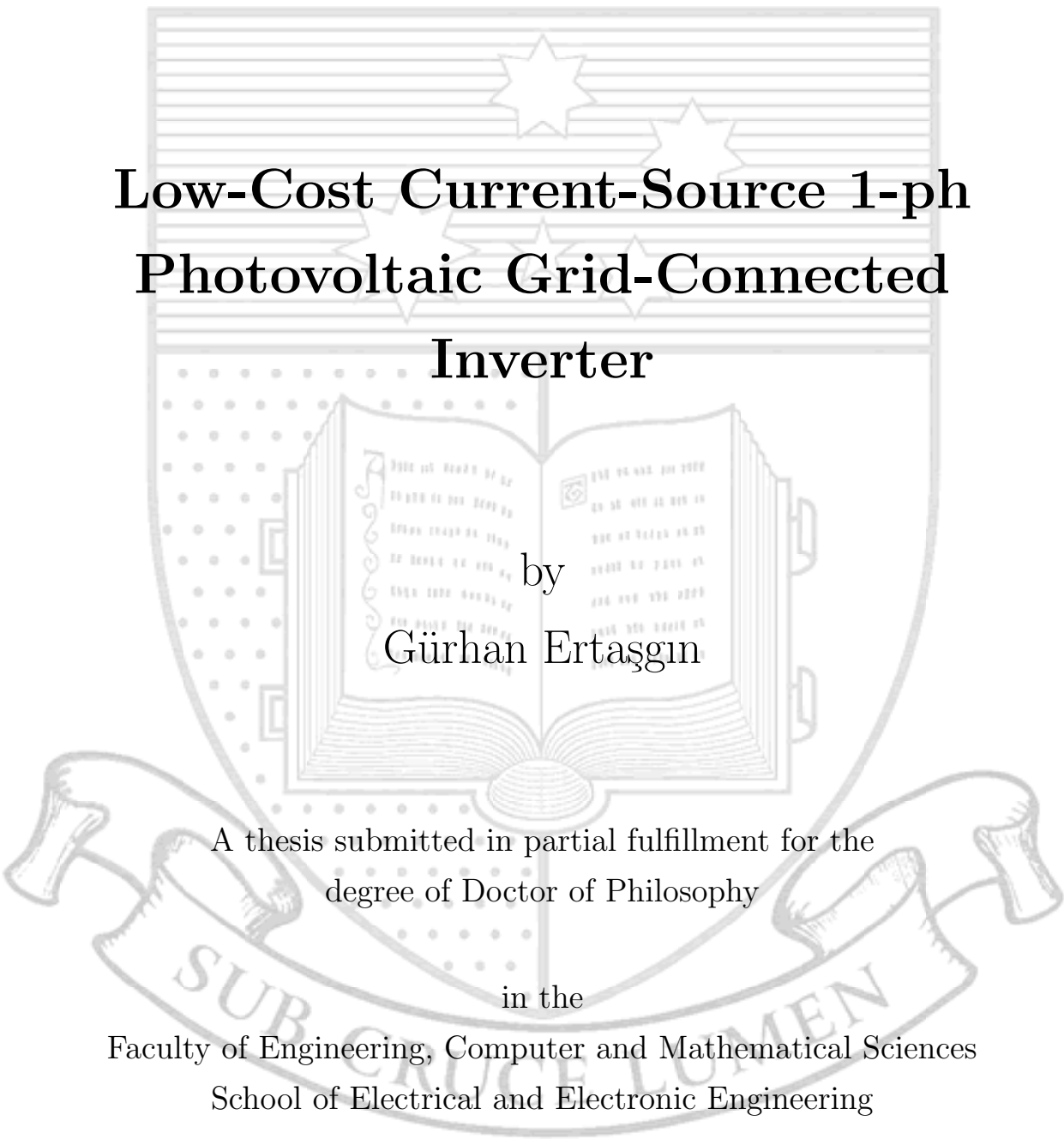


THE UNIVERSITY OF ADELAIDE

The background of the cover features a large, faint watermark of the University of Adelaide crest. The crest is a shield with a star at the top, a book in the center, and a banner at the bottom with the motto 'SUB CRUCE LUMEN'.

Low-Cost Current-Source 1-ph Photovoltaic Grid-Connected Inverter

by
Gürhan Ertuşın

A thesis submitted in partial fulfillment for the
degree of Doctor of Philosophy

in the

Faculty of Engineering, Computer and Mathematical Sciences
School of Electrical and Electronic Engineering

August 2010

Dedicated to my brother, Ahmet Bülent Ertaşgın

CONTENTS

Abstract	ix
Statement of Originality	x
Acknowledgements	xi
List of Figures	xiv
List of Tables	xix
Abbreviations	xxi
Physical Constants	xxiii
Symbols	xxv
1 Introduction	1
1.1 Renewable Energy Sources	1
1.2 Power Electronics Control	3
1.2.1 Stand-Alone and Grid-Connected Inverters	3
1.3 Grid-Connected Inverter Topologies	4
1.3.1 Voltage Source Inverters	4
1.3.2 Current Source Inverters	5
1.4 Technical Requirements	6
1.4.1 Total Harmonic Distortion	6
1.4.2 Power Factor	7
1.5 Literature Review of CSIs	8
1.5.1 Line-Commutated CSI	8

1.5.2	Self-Commutated CSI	9
1.5.3	Soft-Switched CSI	10
1.5.4	Three-Phase CSI	11
1.6	Research Gap	13
1.6.1	Original Contributions	14
1.7	Thesis Layout	15
2	PV Array Models	17
2.1	Background and PV Module Modelling	17
2.1.1	Non-linear Model	19
2.1.2	Piecewise Linear Model	21
2.1.3	Rectangular Model	22
2.1.4	Irradiance and Temperature Curves with Normalisations	22
2.2	Experimental Testing	24
2.2.1	Dark I-V method	25
2.3	Conclusions	26
3	Energy Storage	27
3.1	Energy Storage Requirement	27
3.2	Current/Voltage Ripple Calculation	30
3.2.1	Effect of Energy Storage on Current/Voltage	31
3.3	PV Power Loss Calculations	33
3.3.1	PV characteristics	34
3.3.2	Average Power Reduction	35
3.4	Application Examples	37
3.5	Summary	38
4	Fundamental Analysis	39
4.1	Proposed Concept	39
4.2	Ideal Current-Source Grid-Connected Inverter	41
4.2.1	Simulation Model	43
4.3	Fundamental Operation of the CSI	44
4.3.1	Idealised Waveforms and Analysis	44
4.3.2	Selection of PV Array to Grid Voltage Ratio	46
4.3.3	Effect of Energy Storage	47
4.3.4	Effect of Modulation Index	50
4.3.5	Effect of Irradiance	56
4.4	Summary	60
5	Low-Pass Filter Design	61
5.1	Low-Pass Filter Design	61
5.1.1	Design Criteria	62
5.1.2	Filter Resonance and Damping	63
5.1.3	Filter Normalisations	64
5.1.4	Filter Configurations	65

5.2	Analysis of Low-Pass Filter with Proposed CSI	68
5.2.1	Phase Advance	70
5.3	Design Trade-Offs	74
5.3.1	Effect of C_n Variation	74
5.3.2	Effect of f_c Variation	75
5.3.3	Effect of Q Variation	76
5.3.4	Summary of Effects of Variations	77
5.4	Summary	77
6	160 W Inverter Simulation and Test Results	79
6.1	Proposed Inverter Implementation	80
6.1.1	Inverter Simulation	80
6.1.2	Inverter Control	80
6.2	Experimental System	83
6.2.1	First CSI Prototype	84
6.2.2	Verification of the First CSI Prototype	85
6.2.3	Second CSI Prototype	87
6.2.4	Verification of the Second CSI Prototype	88
6.3	Performance Analysis of the Second Prototype	90
6.3.1	Modulation Index and Irradiance Adjustments	90
6.3.2	Total Harmonic Distortion	92
6.3.3	Power Factor	93
6.3.4	Efficiency	94
6.4	Feedforward Implementation and Results	97
6.4.1	Feedforward Compensation Control	97
6.4.2	Proof of Feedforward Implementation	98
6.5	Summary	100
7	Design and Simulation of a Higher Power Grid-Connected Inverter	101
7.1	Photovoltaic Array	102
7.1.1	Selection of Solar Array Voltage	102
7.1.2	PV Array Arrangement	102
7.2	DC Link Inductor	104
7.2.1	Required Energy Storage Assumption	104
7.3	Switching Component Ratings	106
7.4	Low-Pass Filter Design	107
7.5	System Simulation	108
7.5.1	Simulation Procedure	108
7.5.2	Voltage and Current Waveforms	110
7.5.3	Total Harmonic Distortion	112
7.5.4	Power Factor	113
7.5.5	Efficiency	114
7.6	Summary	119
8	Conclusion	121

8.1	Background	121
8.2	Key Results	122
8.3	Future Work	124
A	DC Link Inductor Design	125
A.1	Inductor Design for 160 W CSI	125
A.1.1	Inductor Volume Calculations	126
A.1.2	Inductor Airgap and Windings	126
A.1.3	Packing Factor	127
A.1.4	Copper Loss	128
A.2	Experimental Results	130
A.3	Conclusion	133
B	Design Schematics and Controller Code	135
B.1	Design Schematics	135
B.2	Microcontroller Code	139
	Bibliography	145

Abstract

This research investigates a complete analysis and investigation of a single-phase currentsource (CSI) grid-connected inverter topology that is based on a photovoltaic array as a supply and a DC link inductor acting as a constant-current source. The proposed low-cost system is implemented using an open-loop control to prove the concept. Then a well-known feedforward compensation control is implemented to achieve acceptable total harmonic distortion of the inverter output current. A single boost switch (based on a switched-mode rectifier) has a duty-cycle that is modulated sinusoidally at the mains (grid) frequency such that it produces an output current that appears a full-wave rectified sinewave that is synchronised to the grid voltage. Additionally, a H-bridge inverter circuit and a capacitive-inductive low-pass grid filter is used to unfold, filter and feed the sinusoidal output current into the grid.

A number of detailed PV array models are studied and used in the simulations. The relationship between the PV array output ripple and the DC link energy storage (element) for single-phase grid-connected inverters is analysed. The “balanced” ripple definition is introduced to estimate the PV array output power reduction due to ripple.

The proposed grid-connected CSI topology is idealised which ignores : component losses, voltage drops, PWM switching and low-pass output filter resonance effects. Normalised simulations are carried out to investigate DC link energy storage, modulation index and irradiance variation effects with an emphasis on meeting the power factor (PF) and total harmonic distortion (THD) grid requirements.

The low-pass grid filter optimisation for the proposed topology is studied showing a trade-off between the output current THD, power loss, and quality factor. A 160 W inverter is implemented and a set of comprehensive test results obtained to verify the simulations using open-loop and feedforward compensation control. To conclude, a 1.2 kW grid-connected inverter based on the proposed low-cost topology was designed and simulated. Its simulated efficiency of 95% was higher than that of the 160 W inverter.

Statement of Originality

This work contains no material which has been accepted for the award of any other degree or diploma in any university or other tertiary institution and, to the best of my knowledge and belief, contains no material previously published or written by another person, except where due reference has been made in the text.

I give consent to this copy of the thesis, when deposited in the University Library, being available for loan, photocopying and dissemination through the library digital thesis collection, subject to the provisions of the Copyright Act 1968.

I also give permission for the digital version of my thesis to be made available on the web, via the University's digital research repository, the Library catalogue, the Australasian Digital Thesis Program (ADTP) and also through web search engines, unless permission has been granted by the University to restrict access for a period of time.

Signed:

Date:

Acknowledgements

I am especially grateful to my supervisor Assoc. Prof. Nesimi Ertuğrul for his guidance, insightful conversations and encouragement. I am also sincerely grateful to my supervisor Dr. Wen L. Soong whose constant guidance, support, encouragement, help and advice kept me going in the right direction during the course of my postgraduate studies. It has been very stimulating and enjoyable to work with them. I acknowledge the financial support of the University of Adelaide with the Divisional Scholarship.

I thank all the members of the department and especially the members of the “Power Electronics and Control Group” for their friendliness and help over the years. I would like to thank Dr. David M. Whaley, Dr. Gene S. Liew and Dr. Jingwei Zhu.

I would also like to thank Stuart Brand, Ian Linke, Bernard Dumuid and Brandon Pullen for their help in the power electronics laboratory during my research. I thank Pavel Simcik and Rainer Weydert for their help for the microcontroller programming and Rose-Marie Descalzi for her help and support. I thank Dr. L. Bülent Gün for his encouragement and advices.

This thesis would not have been possible without the love and support of my lovely wife, Nihan Ertasgın and my brother A. Bülent Ertasgın. I am grateful to them and appreciate their continuous encouragement, endless support and understanding during my studies.

PUBLICATIONS

- [1] G. Ertasgin, David M. Whaley, N. Ertugrul, Wen L. Soong, “Implementation and performance evaluation of a low-cost current-source grid-connected inverter for PV applications,” *Proc. IEEE Sustainable Energy Technologies Conf., (ICSET '08)*, 24-27 Nov. 2008, pp. 939-944.
- [2] G. Ertasgin, David M. Whaley, N. Ertugrul, Wen L. Soong, “Analysis and design of energy storage for current-source 1-ph grid-connected PV inverters,” *Proc. IEEE Applied Power Electronics Conf., (APEC '08)*, 24-28 Feb. 2008, pp. 1229-1234.
- [3] G. Ertasgin, David M. Whaley, N. Ertugrul, Wen L. Soong, “A current-source grid-connected converter topology for photovoltaic systems,” *Proc. Australasian Universities Power Engineering Conf., (AUPEC '06)*, 10-13 Dec. 2006.
- [4] David M. Whaley, G. Ertasgin, N. Ertugrul, Wen L. Soong, J. Darbyshire, H. Dehbonei, Chem V. Nayar, “Investigation of a low-cost grid-connected inverter for small-scale wind turbines based on a constant-current source PM generator,” *Proc. IEEE Industry Electronics Conf., (IECON '06)*, 7-10 Nov. 2006, pp. 4297-4302.

LIST OF FIGURES

1.1	<i>Block diagram of a typical wind turbine power conditioning system.</i>	2
1.2	<i>PV cell, module and array structures.</i>	2
1.3	<i>Stand-alone and grid-connected systems.</i>	4
1.4	<i>Single-phase voltage and current-source inverters.</i>	5
1.5	<i>Early CSI inverter topology.</i>	8
1.6	<i>A single-phase H-bridge CSI using series diode-transistor arrangement.</i>	9
1.7	<i>GTO based H-bridge current-source inverter.</i>	10
1.8	<i>Early grid-connected CSI topology.</i>	10
1.9	<i>Thyristor H-bridge soft-switched current-source inverter topology.</i>	11
1.10	<i>Current-source grid-connected wind inverter topology.</i>	12
1.11	<i>Current-source three-phase inverter topology.</i>	12
1.12	<i>Current-source boost inverter topology.</i>	13
1.13	<i>Proposed grid-connected inverter topology.</i>	14
1.14	<i>Thesis layout consists of chapters.</i>	16
2.1	<i>Typical I-V curve of a PV module.</i>	18
2.2	<i>Voltage variations, reference to (a) irradiance and (b) temperature at MPP.</i>	23
2.3	<i>Non-linear I-V curves for various irradiance and temperature values.</i>	24
2.4	<i>Dark I-V block diagram.</i>	25
2.5	<i>The non-linear model I-V and P-V curves including dark I-V results.</i>	26
3.1	<i>Block diagram of the power reduction.</i>	28
3.2	<i>Common single-phase PV inveter topologies.</i>	29
3.3	<i>Single-phase current-source GCI.</i>	30
3.4	<i>Demonstration of energy buffering.</i>	32
3.5	<i>PV array output current variation diagram.</i>	34
3.6	<i>Normalised power-current curves.</i>	35
3.7	<i>Definition of centred (a) and balanced assumptions (b) for ΔI.</i>	35
3.8	<i>Average power reduction versus voltage and current ripples.</i>	36
4.1	<i>Grid-connected CSI showing previous wind and proposed PV applications.</i>	40

4.2	<i>Ideal single-phase current-source grid-connected inverter.</i>	42
4.3	<i>Grid-connected inverter simulation circuit using PSIM.</i>	43
4.4	<i>Ideal waveform flow diagram of the GC CSI at MPP.</i>	45
4.5	<i>PV array power reduction curves due to temperature.</i>	47
4.6	<i>Normalised output power vs. energy storage for various PV array models.</i>	50
4.7	<i>PV array voltage vs. current curves showing operating points.</i>	51
4.8	<i>Effect of modulation index changes on PV array operating point.</i>	53
4.9	<i>THD and power factor as a function of normalised inverter output power.</i>	56
4.10	<i>THD and PF curves using different energy storage and control approaches.</i>	59
5.1	<i>Common grid-connected inverter low-pass filter types.</i>	62
5.2	<i>Parallel-damped CL type low-pass filter.</i>	63
5.3	<i>Power loss and THD contours of 5%, for filter configurations.</i>	67
5.4	<i>The unfolding circuit output current without and with phase advance.</i>	71
5.5	<i>Analytical phase advance φ and its corresponding phase difference α.</i>	72
5.6	<i>The CSI output power vs. THD, PF and P_d by changing C_n.</i>	75
5.7	<i>The CSI output power vs. THD, PF and P_d by changing f_c.</i>	76
5.8	<i>The CSI output power vs. THD, PF and P_d by changing Q.</i>	76
5.9	<i>Damping resistance power loss for several THD values.</i>	77
6.1	<i>Inverter circuit simulation using PSIM.</i>	80
6.2	<i>MPPT algorithm flow diagram using perturb-and-observe method.</i>	81
6.3	<i>Simplified behavioural flow diagram of the microcontroller operation.</i>	83
6.4	<i>Measured PWM signals from controller and SCR pair's drive pulses.</i>	83
6.5	<i>Photo of the CSI prototypes.</i>	84
6.6	<i>Grid-connected CSI test arrangement.</i>	85
6.7	<i>Simulated and measured resistive load current waveforms.</i>	86
6.8	<i>Comparison of the inverter output current waveforms.</i>	87
6.9	<i>Simulated and measured CSI output voltage and current.</i>	89
6.10	<i>Simulated and measured CSI input and output currents.</i>	90
6.11	<i>Simulated and measured CSI input (P_{PV}) and output (P_G) powers.</i>	91
6.12	<i>Simulated and measured CSI THD as a function of output power.</i>	93
6.13	<i>Simulated and measured CSI power factor as a function of output power.</i>	94
6.14	<i>Simulated and measured CSI efficiency as a function of output power.</i>	95
6.15	<i>Calculated rated loss breakdown of the 160 W prototype.</i>	96
6.16	<i>Measured WS input and output currents at 40% m_A.</i>	99
7.1	<i>CSI circuit diagram showing voltage, current values and the voltage drops.</i>	102
7.2	<i>PV array simulation model which consists of six series 4-diode models.</i>	103
7.3	<i>I-V and P-V curves of the 1.2 kW PV array.</i>	104
7.4	<i>Inductor design trade-off graph.</i>	105
7.5	<i>Proposed 1.2 kW inverter topology showing component ratings.</i>	106
7.6	<i>PSIM simulation model of the 1.2 kW CSI using FFD control.</i>	109
7.7	<i>Simulated CSI output voltage and current waveforms.</i>	111
7.8	<i>Simulated 4 kHz PWM switching effect on the output current waveforms.</i>	112

7.9	<i>Simulated CSI total harmonic distortion as a function of output power.</i>	113
7.10	<i>Simulated CSI power factor as a function of output power.</i>	114
7.11	<i>Simulated CSI efficiency as a function of output power.</i>	115
7.12	<i>Designed higher power CSI loss breakdown as a function of output power.</i>	118
7.13	<i>Simulated loss pie chart of the designed grid-connected CSI.</i>	119
A.1	<i>Dimensions for the designed inductor.</i>	126
A.2	<i>Grid-connected CSI test arrangement.</i>	129
A.3	<i>Measured inductance of the two different DC link inductors.</i>	130
A.4	<i>Iron loss vs. coil current and voltage.</i>	131
A.5	<i>The PV array output and the waveshaper input waveforms.</i>	131
B.1	<i>Master file of the PCB design.</i>	135
B.2	<i>The CSI circuit schematic.</i>	136
B.3	<i>Microcontroller and its connections.</i>	137
B.4	<i>The input current and voltage sensors.</i>	138
B.5	<i>The output current and voltage sensors.</i>	138
B.6	<i>PCB layout of the proposed inverter.</i>	139

LIST OF TABLES

1.1	<i>Current Harmonic Limits</i>	7
2.1	<i>Specifications of the 80 W BP Solar BP380U module.</i>	19
2.2	<i>PV simulation models for the BP380U PV module.</i>	20
2.3	<i>Parameter values of the PV module models under nominal conditions.</i>	21
2.4	<i>Effect of different normalisations on the I-V and P-V curves.</i>	23
3.1	<i>Grid-connected PV VSI and CSI examples based on balanced method.</i>	37
4.1	<i>Ideal and non-ideal components of the proposed inverter.</i>	41
4.2	<i>Simulation model parameters of the simplified GC CSI.</i>	44
4.3	<i>Normalised ideal GC CSI waveforms as a function of energy storage.</i>	49
4.4	<i>Rectangular PV array model as a function of modulation index.</i>	52
4.5	<i>4-diode PV array model results as a function of modulation index.</i>	55
4.6	<i>Normalised ideal GC CSI waveforms as a function of irradiance.</i>	57
5.1	<i>Resistive damping of second-order CL filter configurations.</i>	66
5.2	<i>The normalised output currents of the CSI and their FFT spectrums.</i>	69
5.3	<i>The normalised output currents of the CSI with α.</i>	73
6.1	<i>First inverter prototype semiconductor properties.</i>	84
6.2	<i>Parameters of the two CSI prototypes.</i>	85
6.3	<i>Optimised inverter prototype semiconductor properties.</i>	88
6.4	<i>Inverter output filter types and parameters.</i>	92
6.5	<i>Measured output currents of the CSI and their FFT spectrums.</i>	99
7.1	<i>Summary of the proposed 1.2 kW PV array properties.</i>	103
7.2	<i>Parameters of the inductor for the 1.2 kW PV CSI.</i>	105
7.3	<i>The designed higher power inverter component summary.</i>	107
7.4	<i>Low-pass output filter component values and its parameters.</i>	108
7.5	<i>Simulation model parameters of the designed higher power CSI.</i>	110
7.6	<i>Simulated loss calculation summary at the rated output power.</i>	116

A.1	<i>Parameters of the two inductors for the proposed CSI.</i>	129
A.2	<i>160 W inductor measured results.</i>	132

ABBREVIATIONS

AC	Alternating Current
AS	Australian Standards
CC	Constant Current
CCS	Constant Current Source
CL	Capacitive-Inductive
CSI	Current-Source Inverter
CWS	Current Waveshaper
DC	Direct Current
ESR	Equivalent Series Resistance
FC	Filter Configuration
FFD	Feedforward
GC	Grid-Connected
GCI	Grid-Connected Inverter
I-V	Current vs. Voltage
LC	Inductive-Capacitive
LCL	Inductive-Capacitive-Inductive
MLT	Mean Length per Turn
MPP	Maximum Power Point
MPPT	Maximum Power Point Tracking

OL	Open-Loop
PF	Power Factor
PM	Permanent Magnet
PV	Photovoltaic
P-V	Power vs. Voltage
PWL	Piecewise Linear
PWM	Pulse Width Modulation
T	Thyristor
THD	Total Harmonic Distortion
UC	Unfolding Circuit
VSI	Voltage-Source Inverter
WS	Waveshaper

PHYSICAL CONSTANTS

Boltzman constant	k	$=$	1.38×10^{-23}	J K^{-1}
Charge on electron	q	$=$	1.602×10^{-19}	C
Permeability of free space (air)	μ_0	$=$	$4\pi \times 10^{-7}$	H m^{-1}

SYMBOLS

a	temperature coefficient of copper	$\%/^{\circ}\text{C}$
A_W	radius value of copper wire	m
A_{WT}	total winding area	m^2
B	flux density	T
C	capacitance	F
C_{DC}	DC link capacitor	F
C_F	filter capacitor	F
C_{PV}	PV array output capacitor	F
d	duty cycle	%
E	energy storage	J/W
E_0	average energy storage	J
f_1	grid (inverter fundamental) frequency	Hz
f_c	cutoff frequency	Hz
f_R	resonant frequency	Hz
f_{sw}	switching frequency	Hz
g	airgap	m
G	irradiance	W/m^2
g_E	equivalent gap	m
g_T	total gap	m

H_1	the rms value of the first harmonic	V or A
H_n	the rms value of the n^{th} harmonic	V or A
I_0	current at the maximum power	A
I_B	base current	A
i_G	inverter output or grid current	pu
I_G	grid current (fundamental)	pu
i_{IN}	waveshaper input current	pu
i_{IN}^*	desired PV array output current	A
i_L	inductor current	A
i_{L-CC}	inductor current (constant-current)	A
$i_{L-Clipped}$	inductor current (clipped)	A
i_{L-FFD}	inductor current (feedforward control)	A
i_{L-MPP}	inductor current (MPP)	A
I_{L0}	nominal PV array output current (constant)	A
i_{L-OL}	inductor current (open-loop control)	A
i_{OUT}	waveshaper output current	pu
i_{PV}	PV array output current	A or pu
I_{rms}	the rms value of distorted current	A
I_{SC}	short circuit current	A
i_{WS-FFD}	waveshaper output current (feedforward control)	A
i_{WS-OL}	waveshaper output current (open-loop control)	A
L	inductor	H
l_C	mean core magnetic path length	m
L_{DC}	DC link inductor	H
L_F	filter inductor	H or pu
m_A	modulation index	% or pu
n	diode ideality factor	
N	number of turns	
N_S	module cell number	
P	active power	W
P_0	rated maximum power	W

P_0	average output power	W
P_{CU}	inductor power loss	W
P_d	damping resistance power loss	W
pF	packing factor	%
p_{IN}	waveshaper input power	W
p_{LOSS}	ripple loss	W
P_{OUT}	inverter output power	W
R_{CU}	coil resistance	Ω
R_D	damping resistance	Ω
R_S	module series resistance	Ω
S	apparent power	V A
T	period	s
V_0	voltage at the maximum power	V
V_B	base voltage	V
V_{dcMAX}	ripple voltage (maximum)	V
V_{dcMIN}	ripple voltage (minimum)	V
V_g	band gap	V
V_G	grid voltage	pu
v_{IN}	inverter input voltage	V
v_{IN}	waveshaper input voltage	pu
v_{IN-CC}	waveshaper input voltage (constant-current)	V
$v_{IN-Clipped}$	waveshaper input voltage (clipped)	V
v_{IN-MPP}	waveshaper input voltage (MPP)	V
$V_{L,F}$	applied voltage to the filter inductor	pu
V_{OC}	open circuit voltage	V
v_{OUT}	waveshaper output voltage	pu
V_{PK}	peak grid voltage	V or pu
v_{PV}	PV array output voltage	V or pu
V_{UC}	unfolding circuit output voltage	pu
X_L	inductor impedance	pu
Z_0	characteristic impedance	Ω

Z_B	base impedance	Ω
α	phase advance in simulation	deg
α	temperature coefficient of I_{SC}	%/°C
β	temperature coefficient of V_{OC}	V m/°C
Δ	difference	
η	efficiency	%
λ	flux-linkage	V s
ρ	static resistivity	V m/A
φ	phase advance or difference	deg
Φ	flux	V m
ω	angular frequency	rad/s
ω_{cn}	normalised cutoff frequency (relative to f_1)	pu